Optimized Coil Arrangement in Wound Inter-Phase Reactors for High-Power Rectifier Systems

A. Di Gerlando, G.M. Foglia, M.F. Iacchetti, M. Ubaldini

Abstract—**This paper investigates the optimal arrangement of the coils in a wound-type inter-phase reactor to avoid the decreased inductance due to local saturation in the core when operated with high DC current. In theory, the direct currents and the related magnetomotive forces in the two ways of an inter-phase reactor are equal, and this compensation leads one to conclude that the global flux in the yokes is zero. However, the DC currents in the coils produce a significant leakage flux that flows locally in the core. If the coils are not suitably arranged and if the DC current is high, the leakage flux causes local saturation, a drop in the inductance, and noticeable circulation of a triple harmonic current through the reactor. Such a phenomenon is investigated by means of both a simplified field model and 3D magnetostatic simulations. A number of criteria for the arrangement of the coils to improve operation are derived and applied to a real rectification system used in an electrolysis plant. Some in-situ operational measurements of both the original and the improved inter-phase reactor are reported.**

I. Introduction

INTERPHASE reactors (IPRs) have been used for a long time in multiphase rectifiers, and both their design and operation are well established [1],[2]. Currently, much investigation is aimed at reducing the THD of the line current, both by means of active systems or particular configurations. For instance, in [3], a low kVA (0.02 p.u.) active current source injects a triangular current into an IPR. In [4] and [5], a similar triangular current injection is obtained by means of a particular configuration of the system. In [6], a new filter topology is used, where the IPRs perform a double function, acting as decoupling reactors and as filter inductors. In [7] and [8], specially designed line reactors, termed "harmonic blocking reactors", are introduced. Papers [9]-[11] investigate the behavior of a double-tap IPR and the choice of the optimal turn ratio to minimize the THD of the input current.

The most common configuration of an IPR consists of a pass-through bar, where a single bar of large cross section wraps each column of the reactor. This design is used when the IPR has only 2 turns (one for each column); if 4 turns are required, 2 cores are adopted, each one with a pass-through bar design [12]. If more turns are needed, a wound IPR is required. In such a situation, the coil shape, the turn number and the turn pattern are very critical in defining the reactor's operational characteristics. In fact, even if the magnetomotive forces related to DC current of each way roughly equal each other and determine a vanishing flux in the yokes, the leakage flux, which circulates in the window as well as in the external air space, partially flows through the columns and can produce local saturation, especially with high DC currents and when more than one turn per column is used. As it has been proven, the actual inductance of a DC-biased core depends on permeability, which is related to the characteristics of the minor hysteresis loop: the higher the bias, the lower the permeability [13]. Leakage flux determines the local DC-biasing of the material and the decrease in the permeability. As summarized later, more than one turn is often used to reduce the required cross-sectional area of the column, thus achieving the cheapest construction [1]. However, this solution can exacerbate the aforementioned phenomenon, resulting in a significant drop in the inductance and an intolerable increase in ripple in the DC current, especially when operated close to the rated load of the plant. Unfortunately, no detailed information concerning this problem can be found in the literature. The solution proposed in this paper consists of splitting the IPR into several coils and connecting adjacent coils in such a way as to produce small and opposite local DC MMFs. Thus, a local compensation of the DC MMFs can be achieved and the maximum DC flux density in the core, which is mainly due to the global current in each single coil, is drastically reduced. This study arose from the observation of some operational anomalies in a rectifier employed in an electrolysis plant for Zn production, when operated close to the rated current (two twelve-pulse rectifiers, single rated power 42 MVA, DC current 118 kA). The theoretical investigation, based at first on a simplified field model and then on 3D FEM magnetostatic simulations, produced some criteria for an optimized arrangement of the coils in IPRs. A design modification has been proposed on the existing IPR and has been validated by measurements in situ.

II. Problem Description

A. Rectifier configuration.

The rectifying plant consists of two twelve-pulse paralleled groups electrically shifted by 15 deg. The schematic of one twelve pulse group is shown in Fig. 1a: it is a 12-pulse thyristor rectifier, formed by the parallel connection of two 6-pulse double stars with IPR rectifiers. The two stars of each 6-pulse system are connected by a triple-frequency IPR, but, due

The authors are with the Department of Energy, Politecnico di Milano, Via Lambruschini 4, 20156, Milan, Italy (phone +3902239937[22,46,60,95]; e-mail [antonino.digerlando, gianmaria.foglia, matteo.iacchetti, mario.ubaldini]@polimi.it).

to the circuit inductance, the two 6-pulse systems are connected in parallel directly, i.e., without a six-fold-frequency reactor. An autotransformer (not shown in Fig. 1a, connected to the primaries of the rectifier transformers) is used for coarse voltage regulation, whereas fine regulation is performed by the thyristors. The main electrical data of the whole conversion system are displayed in Table I.

TABLE I
MAIN ELECTRICAL DATA OF THE CONVERSION SYSTEM

Power [MVA] of each twelve pulse group	42.5
Primary and secondary voltage, line to line [kV]	20.0/0.526 (*)
DC voltage [V]	356 (**)
DC current $2 \cdot I_{dc}$ [kA] of each twelve pulse group	118

(*) This value corresponds to the highest tap of the regulating autotransformer.
(**) DC voltage refers to no-load operation in ideal conditions that is null commutation angle ($u = 0$) and null fire angle ($\alpha = 0$): $(3/(\pi\sqrt{2})) \cdot 526 = 356$ V.

B. Traditional design procedure for an IPR

Traditionally, the IPR coil (for example, IPR_A in Fig. 1a) is made with two half coils (IPR_{A1}, IPR_{A2} in Fig. 1b), which are connected in such a way that the two DC currents I_{dcA1} and I_{dcA2} (due to the load) generate two opposite magnetomotive forces (MMFs) M_{dc1} and M_{dc2}. Globally, these DC MMFs cancel each other, so that the core is magnetized only by the AC current I_{ac} due to the voltage difference between the star points SP_{A1} and SP_{A2} of the two opposite stars.

According to typical manufacturer practice, the IPR design is carried out as follows:

- the operational data of the DC plant (voltage V_{dc} , current I_{dc}) are known; the AC supply system characteristics are also known (supply voltage V_{ac}, commutation reactance X_c, firing angle of the thyristors); some theoretical relations exist to evaluate the triple-frequency AC voltage V_{IPR} across the IPR (see the chart in Fig. 2);
- based on the desired losses, the peak flux density AC component B_{ac} is chosen (peak value of the equivalent sinusoidal waveform); to limit the losses to approximately 1 W/kg, typical values adopted in 50 Hz grids are $B_{ac} = 0.8$ T or 0.5 T for IPRs at triple and six-fold frequency, respectively ($f = 150$ or 300 Hz); in the case of 60 Hz grids, the values are reduced;
- from the relation $V_{ac} = (2 \cdot \pi/\sqrt{2}) \cdot f \cdot N \cdot B_{ac} \cdot A_{fe}$, the product $N \cdot A_{fe}$ is deduced, where A_{fe} is the core section area and N is the IPR total turn number ($N/2$ on each column);
- to determine N and A_{fe}, empirical criteria are adopted; usually, a maximum value of A_{fe} is fixed, and N is obtained; some manufacturers typically use values for A_{fe} of approximately 800-1600 cm^2; if $N = 2$ or 4, the through-bar solution is adopted, and the IPR has 1 or 2 cores, respectively [12]; if $N > 4$, a wound IPR is adopted;
- the determination of N and A_{fe} is often related to space issues: because the IPR is located in the same tank as the rectifier transformer, a reduction of A_{fe} is desirable.

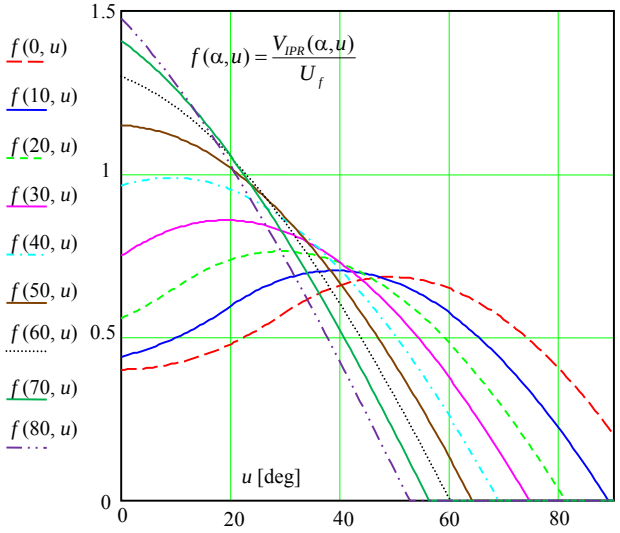

Fig. 2. Typical behavior of the function f(α, u), which is the ratio between the equivalent rms value V_{IPR} of the voltage v_{IPR} across the IPR, and the phase to neutral supply voltage U_f , as a function of the thyristor firing angle α and the commutation angle u. The curves are obtained by the theory in [1].

C. Behavior of a DC-biased core

To understand a number of issues concerning the design of an IPR, it is useful to summarize the behavior of a ferromagnetic core excited by a periodic MMF, which includes both a DC bias M_{dc} and an AC component M_{ac}.

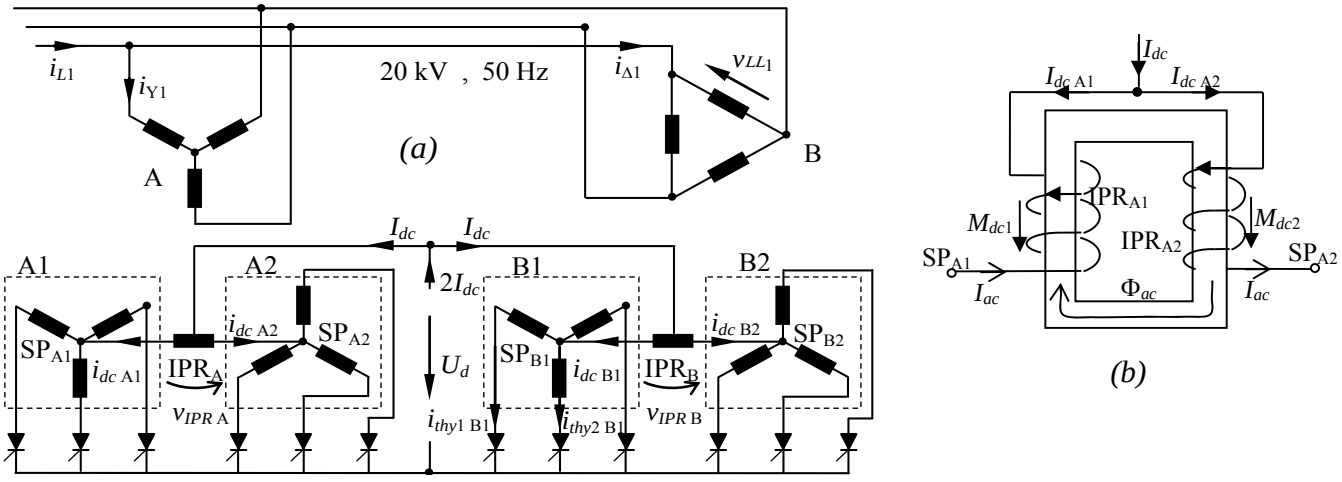

Fig1. (a) Schematic of one twelve pulse rectifier group. IPR_A and IPR_B are the two IPRs. SP are the star points of the stars. (b) Operation of an IPR.

> If only M_{ac} exists and it is not enough to produce saturation, the tip point (H_{ac}, B_{ac}) of the hysteresis loop belongs to the almost linear part of the normal magnetization curve, and the relative apparent permeability $B_{ac}/(\mu_0 H_{ac})$ is approximately 5000-10000. As a consequence, the ferromagnetic circuit has a high permeance, and the coil has a high reactance.

If both M_{ac} and M_{dc} exist and $M_{ac} << M_{dc}$, M_{ac} causes a minor hysteresis loop, which can be approximated with a straight line with a slope much lower than the apparent permeability B_{ac}/H_{ac}. As a consequence, the coil reactance considerably decreases. The center point of the minor loop may not lie on the normal magnetization curve: it is placed so that the resultant current waveform exactly produces M_{dc} [14].

D. *Occurred problem.*

Fig. 1b shows that the MMFs in the two columns due to the DC currents compensate for each other so that a vanishing DC flux is expected in the yokes. However, such compensation only holds true in terms of global quantities. Actually, the coils wound around each column create significant leakage flux whose field lines close through the air, inside and outside the window, as well as through the column. For high DC MMF (as in the case of a turn number greater than one), local saturation in the core can occur. As a consequence, the AC current causes a minor loop with a very low slope, the IPR reactance remarkably decreases, the IPR does not work as intended, and the amplitude of the AC current through it becomes intolerable. This phenomenon is practically negligible in the case of a pass-through bar, but it might become dangerous when $N > 2$, because an increase of N implies both a reduction of A_{fe} and an increase of the DC MMF, which cooperate to increase the local B_{dc} levels.

As detailed in Section VII, this behavior has been clearly observed in an IPR of a rectifier for an electrolysis plant, during operation at a high current level near the rated value. As a result, overheating of the IPR and anomalous voltage drops occurred.

Notice that one of the reasons why such a phenomenon occurred in the present case is the high power of the plant (42.5 MVA). In fact, high power requires that both the voltage and the current are high. A high voltage requires a high value of the product $N \cdot A_{fe}$, thus $N > 2$ is adopted to limit A_{fe}. If the power is lower, the voltage is also lower; thus, $N = 2$ can be adopted, and the MMF is not high enough to cause local saturation.

It should be noted that the aforementioned phenomenon is produced by the local DC biasing caused by the leakage flux, and it is not to be confused with the effect of a global DC bias due to the imperfect balance of the DC MMFs. This last problem is easily avoided by inserting a suitable air-gap in the core, which also allows an almost linear inductance.

The solution proposed here for the aforementioned problem, consists of preserving the original core, splitting the winding of each column into several coils, and performing suitable connections to obtain opposite DC MMFs in adjacent coils on the same column. This way, a local compensation of the MMFs is achieved. However, as will be shown in the next section, the optimal arrangement of the coils should consider both of the columns.

III. Model of the Field in the IPR Core

A. *Main hypotheses.*

The flux density in the IPR core depends on the number and the positioning of the coils wound around the core. Unfortunately, the local nature of the biasing makes an analysis based on simple analytical expressions very difficult. Nevertheless, to give an estimation of such a flux density, a simple field model was investigated.

The model assumes that the two stars are exactly equal to each other, thus a perfect balance between the two ways occurs ($I_{dcA1} = I_{dcA2} = I_{dc}/2$, see Fig. 1b). As previously mentioned, any unbalance due to the unavoidable difference in the two ways can be practically eliminated by inserting a suitable air gap in the core [1]. Moreover, because the aim of the model is to study only the leakage flux and its effects on the flux density in the core, the air gap is not considered in the model.

To reduce the core flux density, the coils on the same column are arranged in such a way that two adjacent coils always produce opposite MMFs. It is assumed that the coils per column are N_c, the column MMF (i.e., the total column current) is I_{tcol}, the total winding height is h_{col}, the coil MMF and the coil height are $M_c = I_{tcol}/N_c$ and $h_c = h_{col}/N_c$, respectively.

The main simplifying hypotheses are as follows:

– the problem is studied in 2D planar XY (infinite dimension Z); the expressions are then integrated along a circumferential line to take into account the cylindrical shape of the core;
– the coils have an infinitesimal thickness;
– the core columns have an infinite height in the Y direction, compared to the Y extension of each coil;
– the core permeability is infinite.

In an IPR, two columns are facing each other, thus the core flux has two contributors, due to the field inside and outside the IPR window, respectively. Moreover, the field inside the window depends on the coil disposition: two facing coils can produce MMF in the same direction, or in opposite directions: in the former case, the two facing coil sides have opposite currents, whereas in the latter case the coil sides have currents flowing in the same direction. The three cases of flux paths are shown in Fig. 3, where red coils produce upward MMFs, and light red coils produce downward MMFs.

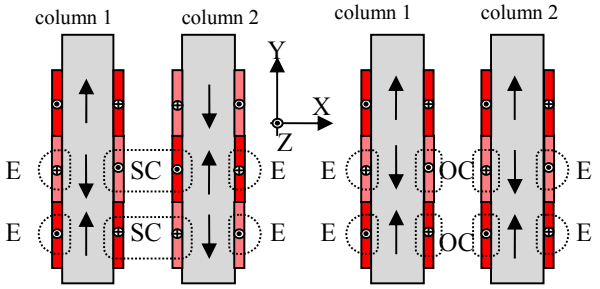

Fig. 3. Types of flux paths in the IPR core. E: outside window field (external field). SC: inside window field, when facing coil sides have currents flowing in the same direction (same current). OC: inside window field, when facing coil sides have currents flowing in opposite directions (opposite current).

B. *Outside window field (external, E).*

For a coil side which stands outside the IPR window, it is assumed that the flux lines are semi-circumferences centered on the coil side center, which extend as far as the coil end (the maximum radius equals $h_c/2$), Fig. 4(a).

The flux line that starts from a generic point, at a distance y from the center, is $\pi \cdot y$ long and is produced by a MMF equal to $2 \cdot y \cdot M_c / h_c$. Hence, the field is independent of the position y, and equals $H_E = (2/\pi) \cdot M_c / h_c$; the flux density is $B_E = \mu_0 \cdot H_E$, and the flux (per unit length in z direction) is $\varphi_E = B_E \cdot h_c/2$; thus, the resulting external flux is

$$\varphi_E = M_c \cdot \mu_0/\pi = (\mu_0/\pi) \cdot I_{tcol} / N_c \, . \qquad (1)$$

The first conclusion is that, to reduce the local core flux density, the coil number N_c must be increased.

C. *Facing coil sides with current in the same direction (SC)*

It is assumed that the flux lines have rectangular shape, starting from the coil center (Fig. 4b).

Due to the infinite permeability of iron, the magnetic voltage drop in the window equals the coil MMF, and all the flux lines have the same length, which is equal to the window width w_w. The flux line that starts from a generic point, at a distance y from the center, is produced by an MMF equal to $(2y/h_c) \cdot M_c$. The field depends on the position y, and equals $H_{SC} = 2y/w_w \, M_c/h_c$; the flux density is $B_{SC} = \mu_0 H_{SC}$, and the flux is the integral of the flux density, from 0 to $h_c/2$; thus, currents having the same direction in opposite facing coil sides produce the following flux (per unit length in z direction)

$$\varphi_{SC} = M_c \cdot (h_c/w_w) \cdot \mu_0/4 \, . \qquad (2)$$

D. *Facing coil sides with opposite currents (OC).*

Again it is assumed that the flux lines are rectangular, starting from the coil side center (Fig. 4c)

The flux line that starts from a generic point, at a distance y from the center, is $2y\,(1 + w_w/h_c)$ long, and it is produced by a MMF equal to $2yM_c/h_c$. Thus, the field is independent of the position y and equals $H_{OC} = M_c / (h_c + w_w)$; the flux density is $B_{OC} = \mu_0 H_{OC}$, and the flux (per unit length in z direction) is $\varphi_{OC} = (h_c/2) \cdot B_{OC}$; hence, the flux due to facing coil sides carrying currents in opposite directions is

$$\varphi_{OC} = (\mu_0/2) \cdot M_c / (1 + w_w/h_c) \, . \qquad (3)$$

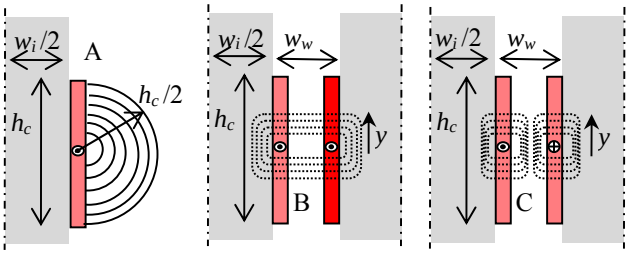

Fig. 4. Field model for the 3 considered fields. A: outside window field. B: inside window field, when facing coil sides have currents in the same direction. C: inside window field, when facing coil sides have opposite currents.

E. *Resulting field in the column.*

To take into account the 3D geometry, the flux per unit length must be multiplied by a corresponding length. It is assumed that the external flux passes through an annular region, whose inner and outer radii are $w_i/2$ and $(w_i + h_c)/2$, respectively (Fig. 5). Therefore, the integration line length is $L = (w_i + h_c/2)\,\pi$ (dotted line in Fig. 5). Moreover, concerning the share of the global leakage flux from the two contributors (internal and external), it is further assumed that 15% of the integration line is related to the internal flux. Thus, the total core flux is

$$\Phi_i = L\,(0.85\,\varphi_E + 0.15\,\varphi_C), \qquad (4)$$

where φ_C can be φ_{SC} (2) or φ_{OC} (3). By dividing (4) by the core section area, the core flux density is derived:

$$B_i = \Phi_i / (w_i^2\,\pi/4) \, . \qquad (5)$$

Table II displays the sizes of the considered real IPR, and Table III displays the core flux density obtained from the previous model, when the coils per column are $N_c = 2, 4, 14$.

TABLE II
MAIN SIZES [mm] AND CHARACTERISTICS OF THE CONSIDERED REAL IPR

w_w	w_i	h_{col}	I_{tcol} [kA]
220	360	990	120

TABLE III
CORE FLUX DENSITY OBTAINED FROM THE PROPOSED MODEL

N_c	2	4	14
B_{iSC} [T]	0.502	0.176	0.037
B_{iOC} [T]	0.456	0.175	0.038

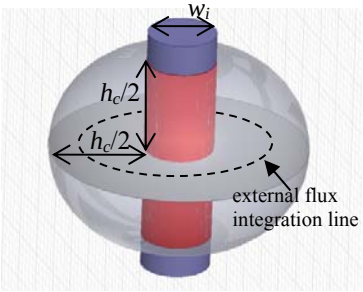

Fig. 5. Flux lines model for the external field.

IV. 3D FEM MAGNETOSTATIC SIMULATIONS RESULTS

Several cases have been simulated. In the first case, each IPR column has a single coil (fed by the current of one star, as in Fig. 1b): in this case, clearly the two facing coil sides have currents in opposite directions. In all the other cases, each IPR column has N_c coils (the considered cases are $N_c = 2, 4, 14$), which can be placed as in the two arrangements shown in Fig. 3 (i.e.: current directions in faced coils can be the same or the opposite). Notice that, to produce opposite MMFs (for the IPR to operate as intended), two adjacent coils on the same column must be fed by different stars: this way, only the DC MMFs oppose each other, whereas the AC MMFs have the same direction. All the considered cases are shown in Fig. 6, where the coils of one star are colored in red, and those of the second star are colored in blue. Moreover, in order to depict the different directions of the currents, a dark color produces an upward MMF, a light color a downward one.

> Due to the symmetry, only half an IPR has been modeled.

In all the cases, the flux density magnitude is plotted on the symmetry plane *xy* ($z = 0$), and the flux density tangential component B_{tan} is evaluated along the mean line of the core, starting from the point half way along the column and moving in a counterclockwise direction (linear coordinate λ along the red line in Fig. 7).

The core is made of 1010 steel.

Fig. 8 shows that in the columns the flux density is uniform throughout the section: therefore, even if the flux density is reported only in one point of the section (the point along the core mean line), such a value can be assumed as the flux density in the whole section.

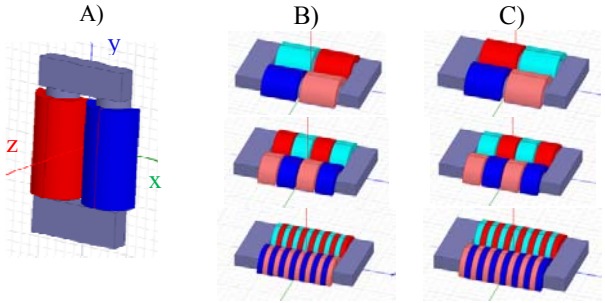

Fig. 6. Analyzed 3D models. A: each IPR column has a single coil. B, C: each IPR column has N_c = 2, 4, 14 coils, which are positioned in such a way that two facing coil sides have currents in the same direction (B) or opposite directions (C).
On the same column, two adjacent coils are fed by different stars (red or blue); a dark color produces an upward MMF, a light color a downward one.

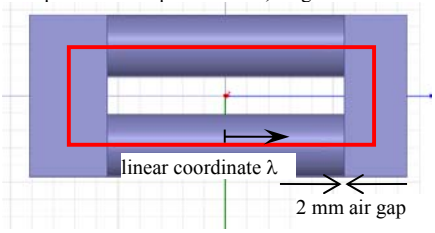

Fig. 7. Core mean line (coordinate λ), along which the flux density is evaluated.

Unlike the analytical model, in the FEM model, the air gap is considered, because (as previously stated) it is often adopted in real IPRs. Similar to typical manufacturer practice, a value of a few mms is adopted (in this case 2 mm per column).

A. IPR column with a single coil.

As discussed in Sec. II-*D*, each DC MMF magnetizes its column, and core saturation occurs.

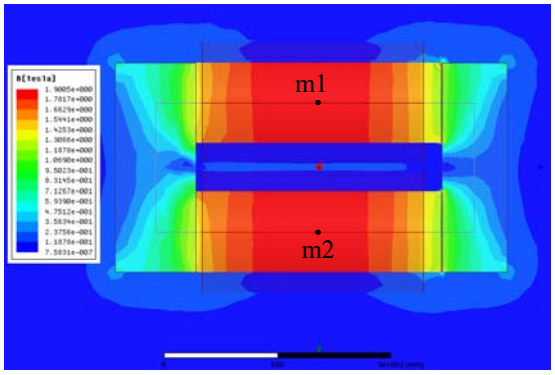

Fig. 8. Flux density of case A) in Fig. 6. Magnitude on the plane $z = 0$.

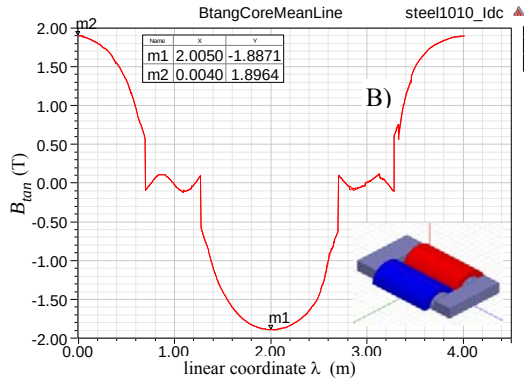

Fig. 9. Tangential component of the flux density of case A) in Fig. 6, along the core mean line.

B. IPR column with N_c coils – coil sides with currents in the same direction (SC).

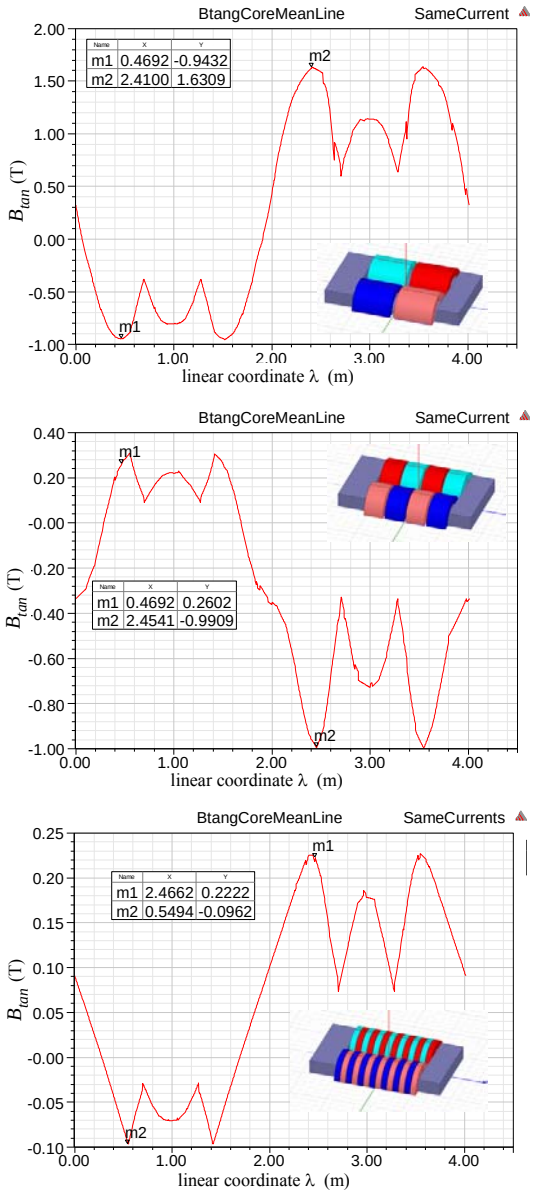

Fig. 10. Flux density tangential component along the core mean line, when each IPR column has N_c coils and facing coil sides have currents in the same

direction.

C. IPR column with N_c coils – coil sides with currents in opposite directions (OC).

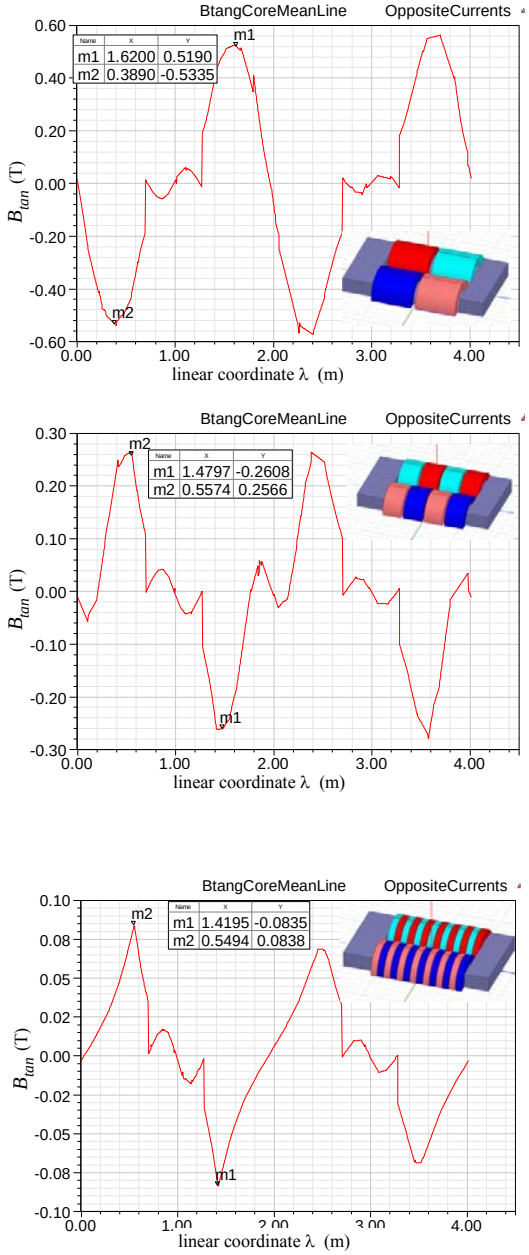

Fig. 11. Flux density tangential component along the core mean line, when each IPR column has N_c coils and facing coil sides have currents in opposite directions.

As predicted in Sec. III-*B*, an increase in the coil number reduces the local flux density inside the core.

Fig. 10 shows that, in the cases of coil sides with current in the same direction (SC), the air gap causes a dissymmetry, where the highest flux density in the upper yoke is much lower than the one in the lower yoke. Moreover, this asymmetry increases the peak flux density (compared to Fig. 11). In light of these results, designs with the same current direction should be avoided.

V. Comparison Between FEM Results and Field Model - Guidelines for the IPR Subdivision

Let us disregard the cases with the same current directions, because the air gap introduces a dissymmetry in the field. In the cases with opposite currents, Table IV displays the core flux density obtained both by the simplified proposed model (results of Table III) and by 3D FEM simulations (Fig. 11), and their ratio.

TABLE IV
Core Flux Density Obtained from the Proposed Model and by FEM

N_c	2	4	14
B_{iOC} [T]	0.456	0.175	0.038
$B_{iOC.FEM}$ [T]	0.52	0.26	0.084
ratio	0.88	0.67	0.45

If N_c is low (as usually occurs), the proposed model gives a fair estimate of the maximum flux density and can be adopted in the first design stage as guidance for the evaluation of N_c.

For a new design of an IPR, an important target could be the minimization of a suitable weighted sum of the copper and iron masses in the IPR. The window section and the core section areas (A_w and A_c) can be related to the DC current (I_{dc}) the tolerable current density (J) and the peak AC component B_{ac} of the flux density by

$$A_w = N I_{dc} / (k_{cu} J) \quad , \quad A_c = V_{IPR} / (N \omega_3 B_{ac}), \qquad (6)$$

where k_{cu} is the copper fill factor, ω_3 is the triple angular frequency and again N is the IPR total turn number ($N/2$ on each column).

Equations (6) show that when N increases, A_w increases, whereas A_c decreases; thus, a minimum exists for any weighted sum of the copper and iron masses. However, the optimization of N must also take into account the constraint of the maximum tolerable B_i. Such a constraint could be stated by using (5), but for an accurate optimization analysis, it is advisable to replace (5) with a 3D FEM model.

VI. Results of Preliminary Circuital Simulations

In order to show the effect of the IPR inductance on the operation of the rectifier, some simulations have been performed by using a circuital model implemented by the Sim-Power-System libraries of Matlab-Simulink. Three cases have been considered, namely:

a) operation at low load (25% of the rated load) and with the unsaturated value of the IPR inductance as estimated by FEM (L_{IPR} = 2.1 mH) (see Fig. 12)

b) operation at medium load (50%) with a value of the IPR inductance (about $0.02 \cdot L_{IPR}$) considerably lower than the unsaturated one (see Fig. 13)

c) operation at high load (80%) and with the unsaturated value of the IPR inductance (see Fig. 14)

The low value of the IPR inductance in case *b* is used in order to consider the presence of two phenomena which occur with the original design of the IPR without coil subdivision:

- saturation of the leakage path closures in the columns, due to the high resultant dc MMF
- high dc polarization and consequent drop of the slope of the

minor hysteresis loop, with a noticeable reduction of the related permeability.

In all the cases, the current waveforms in the thyristor 1 of the star B1, the currents and voltages across the IPR A and B, the line currents and the line voltage just after the autotransformer are shown (see Fig. 1a); the firing angle of the thyristors is set at 15 deg.

Fig. 12 reports the results obtained in the case *a*, which represents the operation with an appropriate value of the IPR inductance, as obtained by either the original design of the IPR at low load (low dc MMF polarization, negligible saturation of the leakage paths on the columns) or by the refined design of the IPR (subdivided coils, then low local dc MMF polarization) both at low or at high load.

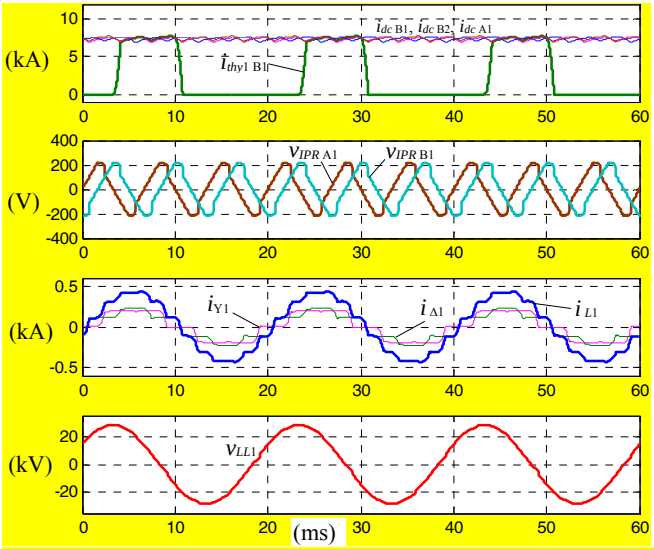

Fig. 12. Simulation results in case *a*: low load with the unsaturated value of the IPR inductance (due to the low load in the original design of the IPR or to the refined design with subdivided coils). The system works properly.

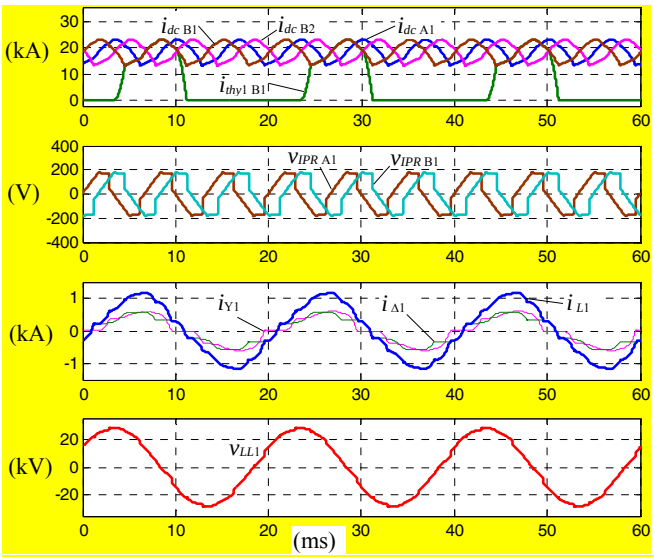

Fig. 13. Simulation results in case *b*: medium load with a low value of the IPR inductance , due to the saturation of the columns in the original design, which is produced by the leakage flux. A noticeable third harmonic ripple exists in the IPR currents and in the thyristor current.

Fig. 13 shows the operation in case *b*, i.e. at medium load level and with a low IPR inductance: this situation happens in the original IPR design when the leakage flux due to the dc current is high enough to saturate the leakage paths inside the columns. In this case, the IPR currents are affected by a noticeable ripple at 150 Hz. Due to this, the line currents differ from the theoretical multi-step square waves.

Fig. 14 refers to case *c*, namely to the operation at high load and with the unsaturated value of the IPR inductance, as it happens in the refined IPR design. Now the third harmonic ripple has disappeared and system operates properly.

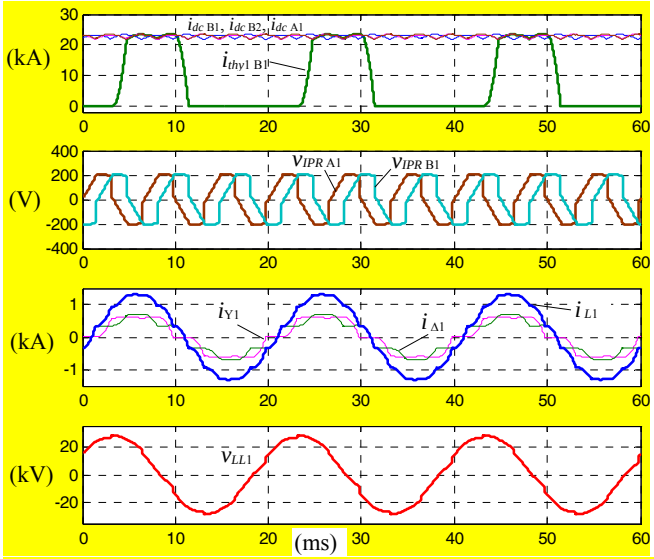

Fig. 14. Simulation results in case *c*: high load with the unsaturated value of the IPR reactance (as in the refined IPR design). The system operates properly, no third harmonic ripple is visible in the thyristor and IPR currents.

VII. Experimental Results of the Original Design

A. Original IPR structure

The scheme of the original IPR structure is shown in Fig. 15, and Fig. 16 shows a picture. Each half coil is made of 14 parallel-connected coils (4 turns per coil, $N = 8$) wound on the same column of the core. Thus, each group of coils around a column behaves as a single coil (see Fig. 9) and a high flux density in the columns is expected.

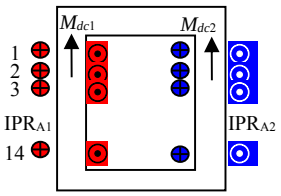

Fig. 15. Original arrangement of the coils in the IPR.

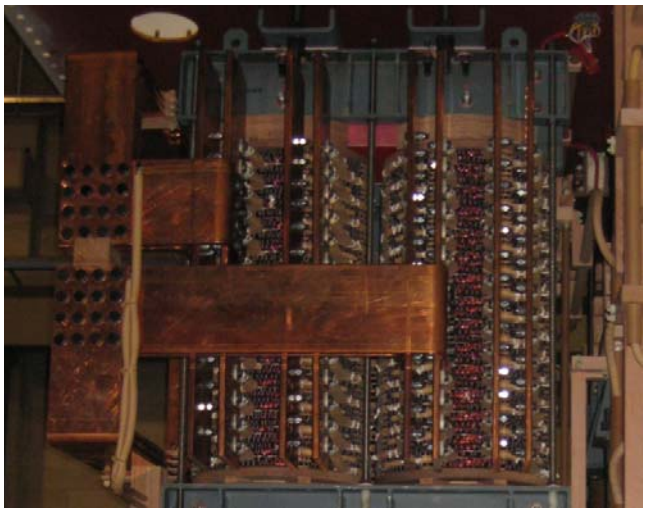

Fig. 16. Picture of the IPR.

B. *Test results*

As a consequence of the original design, the system behaved properly at low load (up to approximately 30% of rated load), but at approximately 60-70% of rated load, as already shown by simulations in Fig. 13, the following anomalies occurred:

- the amplitude of the IPR current ripple (150 Hz) reached 30% of the average value, whereas its design value is a few percentage points;
- the voltage across IPR_A was approximately 2/3 of the voltage across IPR_B, whereas they should be the same;
- the voltage across IPR_B was approximately 2/3 of its design value.

This behavior can be seen in the oscilloscope snapshots displayed in Fig. 17, which show, for both the systems A and B, the IPR DC currents and the voltages across the IPRs, for both low load and 70% of the rated load (I_{dc} = 15.2 kA and I_{dc} = 42.6 kA, respectively).

To fully understand Fig. 17, also refer to Fig. 1a, and take the following information into account:

- CH5 = $v_{IPR\,B1}$, CH6 = $v_{IPR\,A1}$;
- A) low load: CH1 = $i_{dc\,A1}$, CH2 = $i_{dc\,B1}$, CH3 = $i_{thy1\,B1}$, CH4 = $i_{dc\,B2}$; as shown by the oscilloscope labels, CH3 has an offset of 1 V, and CH4 scale is halved with respect to the other channels;
- B) high load: CH1 = $i_{dc\,B1}$, CH2 = $i_{dc\,B2}$, CH3 = $i_{thy1\,B1}$, CH4 = $i_{dc\,A1}$;
- $v_{IPR\,B1}$ phase displacement with respect to $v_{IPR\,A1}$ is 60 deg;
- according to the measurement conventions shown in Fig. 1a, the phase displacements of ripple in $i_{dc\,B1}$ with respect to the other ripples are as follows:
  - 0 deg with respect to the ripple of $i_{thy1\,B1}$;
  - 180 deg with respect to the ripple of $i_{dc\,B2}$;
  - 0 deg with respect to the ripple of $i_{dc\,A1}$, if the operation is correct (low load, ripple with 6-fold frequency);
  - 30 deg with respect to $i_{dc\,A1}$ ripple, if the IPR does not work as intended (high load, ripple with 3-fold frequency).

Fig. 17(a) refers to the operation at low load (approximately 30% of rated load) and should be compared to the corresponding simulation result in Fig. 12: as expected, the currents are quite smooth, and have only a 6-fold frequency ripple. The voltages across the IPRs correctly have equal amplitude, which is near the expected value. Indeed, let us consider the design chart of the ratio between the rms values V_{IPR} of the voltage v_{IPR} across the IPR, and the phase to neutral supply voltage U_f (Fig. 2). By considering the test conditions (commutation angle $u \approx 20$deg, firing angle $\alpha \approx 10$deg), the ratio V_{IPR}/U_f is approximately 0.6, which means that the rms value of V_{IPR} should be about $(V_{LL}/\sqrt{3})\cdot 0.6$, where V_{LL} is the line to line secondary voltage: in the considered test, the tap changer was near the lowest position, and V_{LL} = 325 V. Thus, V_{IPR} should be approximately 113 V. This value is consistent with the rms values indicated by the oscilloscope, which is approximately 95 V (94.6 in one IPR, and 96.5 in the other). It should also be noted that the oscilloscope provides the true rms value of the voltage between the two star points, whereas the value V_{IPR} obtained theoretically is an rms value of an equivalent sinusoid waveform which has the same area as the actual waveform. It can be proven that, when $\alpha>0$, V_{IPR} is higher than the true rms value (by up to 10% or more).

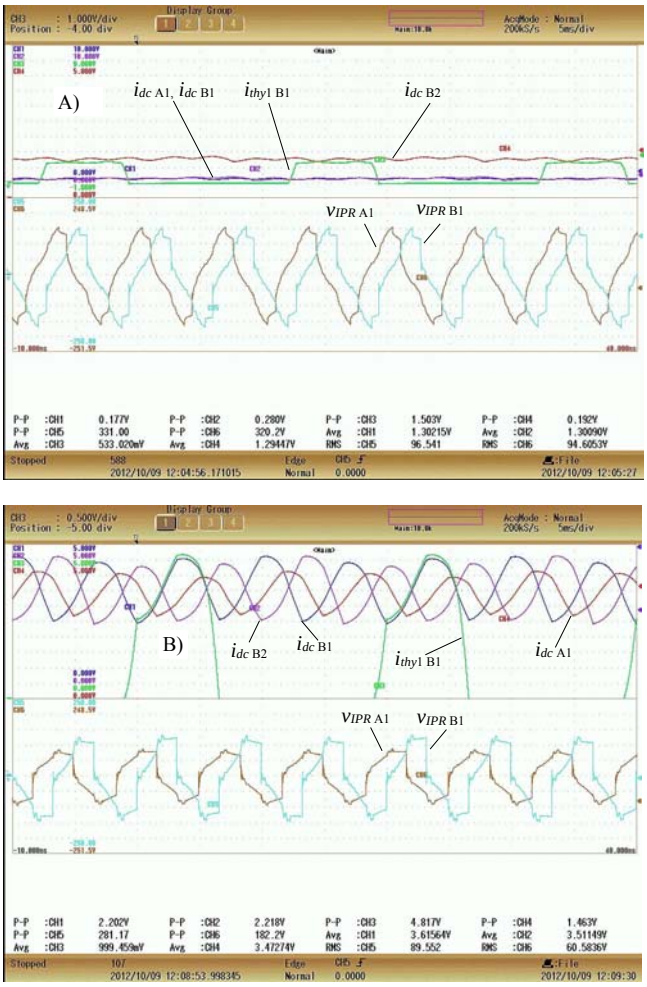

Fig. 17. IPRs currents and voltages with the original IPR design. The current waveform scale is 1 V = 5900A.

Fig. 17b refers to the high load operation (approximately 70% of rated load), and displays the same quantities as Fig. 17a: it

should be compared to Fig. 13. As revealed by simulation results in Fig. 13, an anomalous high ripple appears in the current at 150 Hz (triple frequency), with an amplitude up to 30% of the average value. Indeed, the blue curve in Fig. 17b (CH1, 1 V = 5900A) has an average value of approximately 3.616 V, corresponding to 3.616·5900 = 21.3 kA (I_{dc} = 42.6 kA), and a peak-to-peak value of approximately 2.2 V, corresponding to 13 kA. Thus, the AC amplitude is approximately 30% of the average value, whereas usually it should only be a few percentage points. Moreover, the voltage across IPR_A (60.6 Vrms) is approximately 2/3 of IPR_B (89.6 Vrms), and the voltage across IPR_B is approximately 2/3 of its design value. The test conditions were the same as the previous one ($u \approx 20$deg, $\alpha \approx 10$deg). Thus, again $V_{IPR} \approx (V_{LL}/\sqrt{3})\cdot 0.6$; because the auto-transformer voltage was V_{LL} = 396 V, $V_{IPR} \approx 137$ V, which is not consistent with the rms values indicated by the oscilloscope (89.6 Vrms ≈ 2/3·137); this discrepancy exists even if (as will be explained later) the voltage drop is considered.

C. *Magnetic circuit analysis*

At low load, the IPR current is smooth (Fig. 17(a)): this means that the load inductance (the electrolytic cell's inductance) is enough to smooth the DC current ripple and that the IPR reactance is high enough to limit the AC component (150 Hz) due to the voltage difference between the two star points. The residual 6-fold frequency ripple (300 Hz) is due to the absence of an additional 6-fold frequency IPR between the two 6-pulse systems. Thus, the design value of the IPR reactance seems correct. By contrast, the high ripple that occurs at high load (Fig. 17b) cannot be imputed from a low load inductance because its frequency is 150 Hz (triple frequency). Rather, such a ripple is related to the decrease of the AC reactance relative to the design value. Evidently, in the operation at high load, the high column MMFs produce noticeable leakage flux, which locally saturates the core and reduces the relative permeability.

Moreover, the anomalous high AC current can cause high voltage drops in the circuits; thus, the measured voltage across the IPRs is lower than the expected value. As explained in Sec. I, the reduction in the AC reactance is due to the DC bias: each DC MMF magnetizes its column and saturates the core (Fig. 9). In fact, each coil has 4 turns (total IPR turns, N = 8) and produces a high MMF. According to Sec. I and IV-*C*, the solution is to increase the number of coils and to properly position the coils themselves.

VIII. Experimental Result of the Improved Design

A. *Improved IPR structure*

As indicated by the results of the previous study, the coils have been modified in such a way that two adjacent coils produce opposite MMFs, and moreover, two facing coils have currents in opposite directions. This new arrangement is shown in Fig. 18. Notice that this change was allowed by the structure of each column winding, which was already split into many (specifically 14) small coils (see Fig. 15), such that it only required changing the connections of each coil. Actually, both the FEM simulations and the proposed field model have shown that it is sufficient to split each half coil into 2 or 4 parts to greatly reduce the local core flux density.

Since in this kind of rectifiers the IPR peak voltage is generally low (100 – 300 V) the insulation of the coils in the proposed disposition is not a concern.

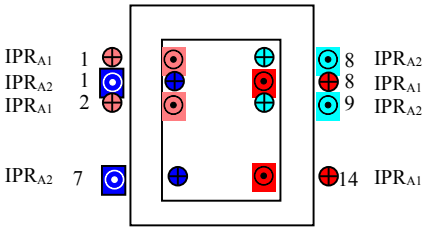

Fig. 18. New arrangement of the small coils in the IPR.

B. *Test results*

The new test results confirmed the correct operation of the system in all of the operating conditions. This can be seen in Fig. 19, which shows the same quantities as Fig. 17 but with the new IPR design. In particular, Fig. 19a and 19b refer to two operating conditions close to the rated load (I_{dc} = 41 kA and I_{dc} = 46 kA, respectively). The experimental waveforms are similar to the simulated ones reported in Fig. 14.

Again, the following information holds for Fig. 19:

- CH5 = $v_{IPR\,B1}$, CH6 = $v_{IPR\,A1}$;
- A): CH1 = $-i_{dc\,B1}$, CH2 = $i_{dc\,B2}$, CH3 = $i_{thy1\,B1}$, CH4 = $i_{thy2\,B1}$
- B): CH1 = $i_{thy1\,B1}$, CH2 = $i_{dc\,B1}$, CH3 = $i_{dc\,B2}$, CH4 = $i_{dc\,A2}$;
- $v_{IPR\,B1}$ phase displacement with respect to $v_{IPR\,A1}$ is 60 deg;
- according to the measurement conventions shown in Fig. 1a, the phase displacements of the $i_{dc\,B1}$ ripple with respect to the other ripples are as follows:
  - 0 deg with respect to the ripple of $i_{thy1\,B1}$;
  - 180 deg with respect to the ripples of $i_{dc\,B2}$ and $i_{dc\,A2}$.

In all cases, the current ripple is very low and has only a 6-fold frequency: the absence of any significant ripple at 150 Hz (triple harmonic) proves that the IPR reactance is correct. Moreover, the rms voltage across the two IPRs is the same and equals 140 V (see Fig. 19). This value is consistent with the predicted value: the auto-transformer voltage was V_{LL} = 443 V, thus V_{IPR} = (443/√3)·0.6 = 153.5 V; the difference is approximately 10%, as previously explained (difference between the rms values of the oscilloscope (true) and the chart (equivalent)).

Regarding the difference between the two IPR voltages in the original design, where the voltage across IPR_A was approximately 2/3 of the voltage across IPR_B, the most credible hypothesis is that the magnetic coupling between the bars and the structural parts might work as a "short-circuited transformer", and might cause a voltage drop in the bars themselves. This phenomenon only occurred in one IPR, because the bar pattern is a bit different in the other IPR. In the original design, this phenomenon was exaggerated by the high level of the AC current component at 150 Hz. On the contrary, in the improved design, such a component is negligible.

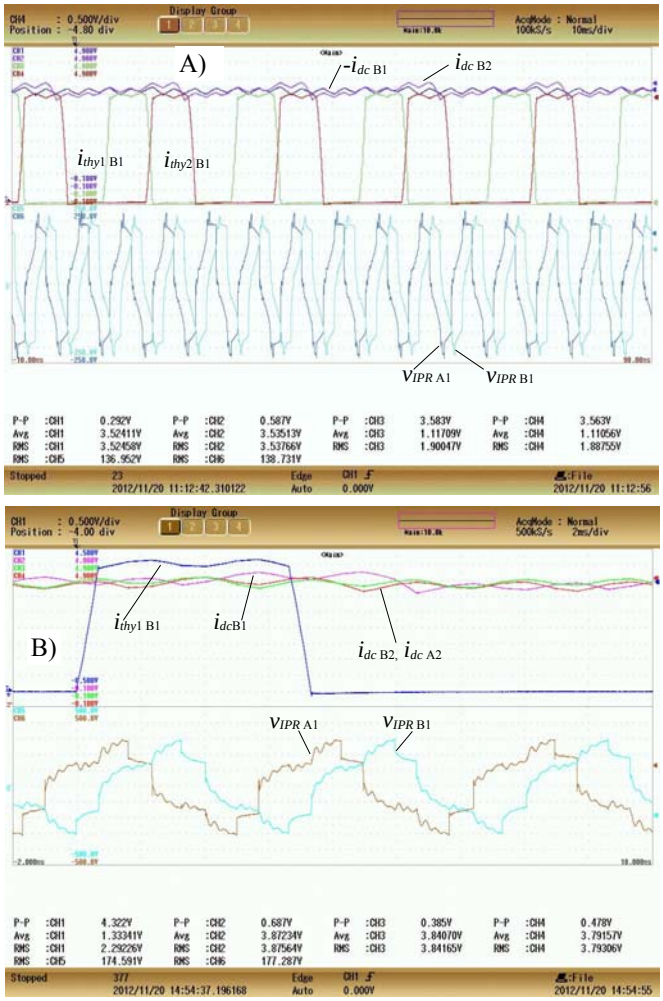

Fig. 19. IPRs currents and voltages, with the new IPR design. Again, the current waveform scale is 1 V = 5900A.

IX. Conclusion

Starting from a real case and using both a simplified analytical model and FEM 3D simulations, the present study shows that in a wound-type IPR, the pattern of the turns has a great impact on the behavior of the system. In particular, if each half-coil is wound on a column of the core, the DC MMFs compensate for each other only globally, whereas they can produce significant leakage flux that locally saturates the columns. As a consequence, the inductance drops and the IPR loses its ability to smooth the AC current. This occurs, for example, when the plant power is high and, as a consequence, the DC current and voltage are high. On the contrary, if the half coils are split in portions, and a proper arrangement is adopted, a local compensation of the MMFs occurs, the core does not saturate, and the IPR behaves in the intended way. The proper arrangement requires that

1) along the same column, the coil MMFs have alternate directions (thus, two adjacent coils on the same column must be fed by different stars);
2) two facing coils (each wound on one column) must produce a MMF with the same direction (the currents in the facing coil sides have opposite directions).

A simple field model has been proposed, which can guide the choice of the number of coils in the first design stage. The higher the coil number, the lower the core local flux density. Usually, 2-4 coils per column are enough to avoid core saturation and to ensure the intended IPR operation. If the IPR current is very high (more than 100 kA), it is advisable to analyze the IPR operation with 3D FEM simulations.

Acknowledgment

The authors thank the technicians and staff of SpecialTrasfo S.p.A. (Trezzano Rosa, Milano, Italy) and Portovesme S.r.L. (Portovesme, Sardinia, Italy) for providing the test data and for their assistance.

References

[1] J.Schaefer, "*Rectifier Circuits, Theory and Design*", John Wiley & Sons Inc. , 1965.

[2] Acosta Orlando N. , "Interphase Transformer for Multiple Connected Power Rectifiers," *Industry and General Applications, IEEE Transactions on* , vol.IGA-1, no.6, pp.423-428, Nov. 1965.

[3] Sewan Choi; Enjeti, P.N.; Hong-Hee Lee; Pitel, I.J., "A new active interphase reactor for 12-pulse rectifiers provides clean power utility interface," *IEEE Trans. Ind. Appl.*, vol.32, no.6, pp.1304,1311, Nov/Dec 1996.

[4] Tanaka, T.; Koshio, N.; Akagi, H.; Nabae, A., "A novel method of reducing the supply current harmonics of a 12-pulse thyristor rectifier with an interphase reactor," *Industry Applications Conference, 1996. Thirty-First IAS Annual Meeting, IAS '96., Conference Record of the 1996 IEEE* , vol.2, no., pp.1256,1262 vol.2, 6-10 Oct 1996

[5] Tanaka, T.; Koshio, N.; Akagi, H.; Nabae, A., "Reducing supply current harmonics," *Industry Applications Magazine, IEEE* , vol.4, no.5, pp.31,37, Sep/Oct 1998.

[6] Pires, V.F.; Silva, J.F.; Anunciada, A., "Twelve pulse parallel rectifier with a new topology for the output low-pass filter," *Power Electronics Specialists Conference, 1996. PESC '96 Record., 27th Annual IEEE* , vol.2, no., pp.1006,1011 vol.2, 23-27 Jun 1996

[7] Rendusara, D.; Von Jouanne, A.; Enjeti, P.; Paice, D.A., "Design considerations for six pulse and twelve pulse diode rectifier systems operating under voltage unbalance and pre-existing voltage distortion with some corrective measures," *Industry Applications Conference, 1995. Thirtieth IAS Annual Meeting, IAS '95., Conference Record of the 1995 IEEE* , vol.3, no., pp.2549,2556 vol.3, 8-12 Oct 1995

[8] Rendusara, D.A.; Von Jouanne, A.; Enjeti, P.N.; Paice, D., "Design considerations for 12-pulse diode rectifier systems operating under voltage unbalance and pre-existing voltage distortion with some corrective measures," *IEEE Trans. Ind. Appl.*, vol.32, no.6, pp.1293,1303, Nov/Dec 1996.

[9] Shiyan Yang; Fangang Meng; Wei Yang, "Optimum Design of Interphase Reactor With Double-Tap Changer Applied to Multipulse Diode Rectifier," *Industrial Electronics, IEEE Transactions on* , vol.57, no.9, pp.3022,3029, Sept. 2010.

[10] Qijun Pan; Weiming Ma; Dezhi Liu, "A practical formula to calculate critical value of the interphase reactor in a six-phase diode rectifier with tap-changer," *Industrial Electronics Society, 2004. IECON 2004. 30th Annual Conference of IEEE*, vol.1, pp.696,699 Vol. 1, 2-6 Nov. 2004.

[11] Pan Qijun; Ma Weiming; Liu Dezhi; Zhao Zhihua; Meng Jin, "A New Critical Formula and Mathematical Model of Double-Tap Interphase Reactor in a Six-Phase Tap-Changer Diode Rectifier," *IEEE Trans. Ind. Electron.,* , vol.54, no.1, pp.479,485, Feb. 2007.

[12] R. Wells, Interphase Transformer in Power Rectifiers, Electrical Review, vol 200, No 7, 1977

[13] R. M. Bozorth, Ferromagnetism, D. van Nostrand, 1951

[14] G.M. Foglia, M. Ubaldini, "D.C. Component in Transformer: Physical Behaviour and Design Features", in *Proc. of ICEM'2004, International Conference on Electrical Machines*, Cracow, Poland, 5-8th September 2004, Conf. Record on CD: Paper N° 54, ISBN 83-921428-0-2.